Dynamic spectrally-enriched LES subgrid-scale modeling for preferential concentration of inertial particles in turbulence

By M. Bassenne, M. Esmaily, D. Livescu†, P. Moin AND J. Urzay

1. Motivation and objectives

Large-eddy simulations (LES) of incompressible turbulence consist of integrating the low-pass-filtered Navier-Stokes equations

$$\frac{\partial \overline{u}_i}{\partial x_i} = 0, \tag{1.1}$$

$$\frac{\partial \overline{u}_i}{\partial t} + \overline{u}_j \frac{\partial \overline{u}_i}{\partial x_j} = -\frac{1}{\rho}\frac{\partial \overline{p}}{\partial x_i} + \nu \frac{\partial^2 \overline{u}_i}{\partial x_j \partial x_j} - \frac{\partial \tau_{ij}}{\partial x_j}, \tag{1.2}$$

which represent the conservation of mass and momentum, respectively. In this formulation, t is the time coordinate, x_i are spatial coordinates, $\overline{u}_i$ are velocity components, $\overline{p}$ is the hydrodynamic pressure, ρ is the density, ν is the kinematic viscosity, and $\tau_{ij} = \overline{u_i u_j} - \overline{u}_i \overline{u}_j$ is the subgrid-scale (SGS) stress tensor. The latter is unclosed and requires modeling since the full-scale velocity u_i, which is the one that bears the full range of spatiotemporal scales in the turbulent flow, cannot be directly obtained from Eqs. (1.1) and (1.2), but requires the costly integration of the unfiltered Navier-Stokes conservation equations.

While Eqs. (1.1) and (1.2) refer to the carrier phase, in particle-laden turbulence an additional set of equations is required to describe the motion of the dispersed phase. In Lagrangian descriptions of the dispersed phase, the trajectory equation

$$\frac{dx_{p,i}}{dt} = u_{p,i} \tag{1.3}$$

is integrated simultaneously with the equation of motion

$$\frac{du_{p,i}}{dt} = \frac{u_i - u_{p,i}}{t_a} \tag{1.4}$$

for every particle. Specifically, Eqs. (1.3) and (1.4) describe the rate of change of the components of the particle position $x_{p,i}$ and particle velocity $u_{p,i}$ along the particle trajectory. In the notation, $t_a = (2/9)(\rho_p/\rho)(a^2/\nu)$ represents the characteristic acceleration time of the particle, with ρ_p and a the particle density and radius, respectively. In writing Eq. (1.4), it is has been assumed that the particle radius is much smaller than the Kolmogorov length scale, that the particle density is much larger than that of the carrier fluid, and that the particle Reynolds number computed using the slip velocity as characteristic velocity is much smaller than unity (Maxey & Riley 1983). Inter-phase coupling terms arising in the momentum conservation equation (1.2) are neglected here by assuming that

† Los Alamos National Laboratory, Los Alamos NM

the mass of the dispersed phase is negligible compared to the mass of the carrier phase, or equivalently, that the characteristic mass-loading ratio $\alpha = (4/3)\pi\rho_p n_0 a^3/\rho \ll 1$ is a small parameter, with n_0 the mean number density of particles.

Of particular interest is the equation of particle motion (1.4), which highlights the closure problem that emerges in LES of particle-laden turbulence. This can be understood by noticing that an appropriate time integration of Eq. (1.4) would require the full-scale carrier-phase velocity u_i – rather than the filtered one $\overline{u}_i$ – in order to describe the exact trajectories of the particles. Inaccurate predictions of some of the dispersed-phase statistics are typically observed when this closure problem is ignored and just $\overline{u}_i$ is employed for the integration of Eq. (1.4) (Marchioli 2017). The weight of the inaccuracies incurred in the predictions is however dependent on the characteristic dimensionless parameters of the problem, and most notably, on the SGS Stokes number $\mathrm{St}_{\mathrm{SGS}}$ in one-way coupled flows, and on the ratio $\alpha/\mathrm{St}_{\mathrm{SGS}}$ in two-way coupled flows, as described in Urzay *et al.* (2014).

Among the dispersed-phase statistics degraded by neglecting the closure problem described above, the inaccurate prediction of the intensity and scales associated with preferential concentration and particle acceleration have been clearly illustrated in Park *et al.* (2017). In particular, the lack of spatiotemporal resolution in LES artificially narrows the amplitude of the particle accelerations and erroneously distributes the particles in the flow field to the extent of misrepresenting the well-known effect of preferential concentration whereby the particles tend to accumulate in flow regions where the strain rate is large (Robinson 1956; Squires & Eaton 1991). Since the inter-phase coupling of momentum that appears in Eq. (1.2) in non-diluted regimes has the form of an effective number density multiplied by the particle acceleration (Ferrante & Elghobashi 2003), it is expected that these discrepancies would directly translate into mistaken predictions of turbulence modulation.

The objective of this report is to formulate a new SGS model in physical space for the carrier-phase velocity u_i to be used in the integration of the equation of particle motion (1.4) in LES of particle-laden turbulence. This investigation builds on some of our previous work (Urzay *et al.* 2014; Park *et al.* 2015, 2017; Bassenne *et al.* 2015, 2017) by proposing a new SGS model based on differential filters that incorporates an spectrally-enriched carrier-phase velocity u_i, which contains scales smaller than the LES grid resolution, thereby enabling the calculation of small-scale phenomena such as the preferential concentration of particles. The new model is dynamic, in that it does not contain tunable parameters, it can be deployed in non-uniform grids, and is applicable to inhomogeneous flows subject to arbitrary boundary conditions.

The remainder of this report is organized as follows. A short review of the different classes of SGS models for particle-laden turbulence is presented in Section 2. In Section 3, the new SGS model formulation is described. Results for the carrier- and dispersed-phase statistics obtained in homogeneous-isotropic turbulence are analyzed in Section 4. Lastly, concluding remarks and suggestions for future work are provided in Section 5.

2. A short survey of SGS models for the motion of inertial particles in turbulence

The SGS modeling endeavor in the present context consists of avoiding to solve the full-scale velocity u_i via costly direct numerical simulations (DNS), which would require prohibitively small control volumes as schematically represented in Figure 1(a). Existing

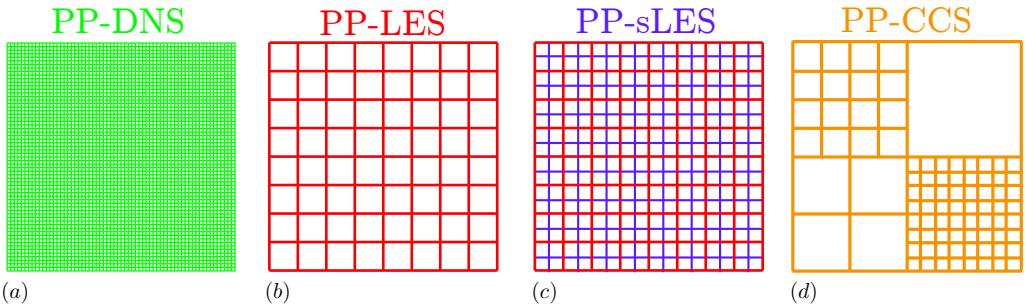

FIGURE 1. Schematics of different computational grids employed in Lagrangian point-particle (PP) numerical simulations of particle-laden turbulence, where the scale of the particle is not resolved by the grid. (a) Direct numerical simulation (DNS) grid that resolves all flow length scales. (b) Large-eddy simulation (LES) grid that resolves fluctuations larger than a filter width. Non-spectrally-enriched SGS models are obtained on the same grid as (b) and do not bear any smaller scales. (c) LES grid (red color online) and refined grid (blue color online) for point–particle spectrally-enriched LES (PP-sLES). The refined grid in (c) uniformly supports smaller scales resulting from the SGS model. (d) Alternative grid for wavelet-based point-particle coherent cluster simulation (PP-CCS) whose control volumes are adapted to particle clusters and resolve all relevant flow length scales around them, while the control volumes away from the clusters remain coarse [see Bassenne *et al.* (2017) for details on the grid-adaptation algorithm].

SGS models for the full-scale velocity u_i can be grouped into two main categories: non-spectrally-enriched point-particle LES models (PP-LES), and spectrally-enriched point-particle LES models (PP-sLES). These are described in Sections 2.1 and 2.2, respectively. Alternatively, Section 2.3 proposes an unexploited approach, namely the point-particle coherent cluster simulation (PP-CCS) based on wavelets. Note that spectral enrichment is primarily used in this report in the sense of augmenting the range of spatial scales, or equivalently, the range of non-zero spectral modes of the velocity field.

2.1. *Non-spectrally-enriched point-particle LES models (PP-LES)*

Oftentimes, SGS models employed in particle-laden turbulence are not spectrally enriched. This category includes approximate-deconvolution models where an approximate inverse filtering is applied to $\overline{u}_i$ in order to generate a model for u_i (Park *et al.* 2015, 2017). However, these models do not recover scales smaller than the LES grid size, and consequently, the spectral content of the modeled velocity u_i has the same wavenumber support as the resolved velocity $\overline{u}_i$, as illustrated in Figure 1(b). A thorough review of approximate-deconvolution models is available in Marchioli (2017). The main limitation of this class of models results from the lack of true reconstruction of SGS motion, whose pernicious effects are particularly noticeable when the interaction of particles with the subgrid scales of turbulence play a central role in the dispersed-phase dynamics. As a result, non-spectrally-enriched point-particle LES models are unable to appropriately capture the size of particle clusters in regimes where preferential concentration is important. In two-way coupled flows, this mismatch is most likely important in SGS-loaded conditions, which are characterized by $\alpha = O(1)$ and $\mathrm{St}_{\mathrm{SGS}} \ll 1$ and where the inter-phase coupling occurs predominantly in the subgrid scales (Urzay *et al.* 2014).

Lagrangian stochastic models partly belong to this category of models and partly to the category of spectrally-enriched models outlined in the next subsection. In these models, the Lagrangian time trace of the local Eulerian flow velocity seen by the particles is spectrally enriched in the time domain – rather than in the space domain – by superposing

random variations to the local value of $\overline{u}_i$ at the particle position. These, in turn, widen the range of accelerations that the particles can be subjected to in a way similar to that observed in DNS, but are generally unable to recover two-point statistics that are necessary to recover preferential-concentration effects and relative dispersion (Minier 2015). Recent modifications of Lagrangian stochastic models, albeit for tracer particles, have been proposed that aim at palliating some of these shortcomings by correlating the random processes in space (Mazzitelli *et al.* 2014).

2.2. *Spectrally-enriched point-particle LES models (PP-sLES)*

In order to circumvent the limitations associated with the lack of fine-grained spatial scales in LES, spectrally-enriched SGS models aim at reconstructing the velocity field on a grid finer that the original LES grid. For instance, a baseline LES grid, along with a reconstructed one to support the enriched scales, are sketched in Figure 1(c). One desirable characteristic that these models should have is the capability of regenerating an spectrally-enriched velocity on the finer grid at a computational cost smaller than that of directly solving Eq. (1.2) on that same grid. Additionally, the challenge of modeling an spectrally-enriched velocity field that resembles turbulence is not free of physical and numerical challenges. In particular, a model of interest for engineering analysis would require to broaden its foundations beyond turbulence theories restricted to idealized scenarios, or beyond numerical schemes only defined on canonical Cartesian uniform grids. Despite these challenges, these are perhaps the most promising models for capturing the full range of eddy scales necessary for preferential concentration to develop in the class of turbulent flows studied here.

SGS models that fall into this category are much less frequently reported in the literature in comparison with approximate-deconvolution or Lagrangian stochastic models (Marchioli 2017). Spectrally-enriched models are typically based on kinematic simulation (Ray & Collins 2014; Murray *et al.* 2016), fractal interpolation (Marchioli *et al.* 2008*a*,*b*) or spectrally-optimized interpolation (Gobert & Manhart 2011). The main difficulties associated with this class of models are the reliance on homogeneous turbulence theory and on tunable parameters whose values outside of the homogeneous turbulence regime are not straightforward to justify theoretically, and the difficulty of generating small-scale turbulence structures that display the correct degree of spatiotemporal correlations (Jiménez *et al.* 1993; Bürger *et al.* 2013; He *et al.* 2017) to which the particles may as well be sensitive during their flight and accumulation into clouds. The new model presented in this report circumvents some of these limitations.

2.3. *Point-particle coherent cluster simulation (PP-CCS)*

An alternative to the traditional LES approaches described above may involve a dynamic refinement of the grid around clusters of particles in a way that precludes or minimizes the need for a SGS model [see Figure 1(d)], as opposed to uniformly coarsening the grid irrespective of the spatial distribution of the dispersed phase. This method, referred here as coherent-cluster simulation (CCS), borrows its philosophy from the extensive body of research on coherent-vorticity extraction and simulation for single-phase turbulence, a methodology that relies on the ability of wavelets to efficiently identify turbulent structures (Schneider & Vasilyev 2010). In a recent work, Bassenne *et al.* (2017) found that wavelets also form an appropriate basis for extracting particle clusters, and that they can be used as a grid-adaptation tool to refine the grid around the clusters. Future research on the translation of this result into an SGS model for particle-laden turbulence may be of interest for establishing the viability of this approach.

3. Description of the spectrally-enriched differential filter (SDF) model

This section describes the spectrally-enriched differential filter (SDF) model proposed in the present work. The SDF model does not have tunable parameters, and is applicable to non-homogeneous flows and non-uniform, non-periodic grids. A single-level reconstruction that corresponds to a grid refinement by a factor of two in each direction is described below. However, the model can be applied recursively to obtain higher levels of refinement. At each reconstruction level, the input velocity to the spectral enrichment algorithm is the modeled velocity obtained from the previous level. The first reconstruction level uses the LES velocity $\overline{u}_i$ as input.

Consider the LES field $\overline{u}_i = u_i^{(2\Delta)}$ described by its nodal values on a grid with local characteristic spacing (2Δ). In general, Δ is an effective grid spacing that may be expressed as a function of its corresponding values per direction as $\Delta = (\Delta_1\Delta_2\Delta_3)^{1/3}$. The SDF-modeled velocity $u_i^{(\Delta)}$, defined on a grid refined by a factor of 2 in all directions, is written as

$$u_i^{(\Delta)} = u_{i,\mathrm{ADI}}^{(\Delta)} + u_{i,\mathrm{SGS}}^{(\Delta)}. \tag{3.1}$$

In this formulation, the velocity field $u_{i,\mathrm{ADI}}^{(\Delta)}$ has scales that mostly range from the integral scale to the LES cutoff 2Δ. Compared to the resolved velocity $u_i^{(2\Delta)}$, the spectral energy of $u_{i,\mathrm{ADI}}^{(\Delta)}$ near the LES cutoff is enhanced by an approximate deconvolution. Conversely, the spectral energy of the velocity field $u_{i,\mathrm{SGS}}^{(\Delta)}$ is mostly populated in the subgrid scales ranging from Δ to 2Δ. As a result, $u_{i,\mathrm{SGS}}^{(\Delta)}$ bears the regenerated scales by spectral enrichment and requires non-trivial modeling. A methodology for computing $u_{i,\mathrm{ADI}}^{(\Delta)}$ and $u_{i,\mathrm{SGS}}^{(\Delta)}$ is described below.

3.1. *Computation of* $u_{i,\mathrm{ADI}}^{(\Delta)}$

The velocity field $u_{i,\mathrm{ADI}}^{(\Delta)}$ originates from an approximately-deconvolved field interpolated on a finer grid. Correspondingly, it is obtained by first applying an approximate-deconvolution model to $u_i^{(2\Delta)}$ on the LES grid and then interpolating the result onto the finer grid.

3.1.1. *Approximate deconvolution on the LES grid*

Given the LES field $u_i^{(2\Delta)}$, an approximately-deconvolved velocity field $u_{i,\mathrm{AD}}^{(2\Delta)}$ is computed in the following way. To benefit from a filtering kernel that is easily applicable to complex geometries and grids, the dynamic differential filter (DF) model of Park *et al.* (2015, 2017) is used in the present study, which provides the expression

$$u_{i,\mathrm{AD}}^{(2\Delta)} = \overline{u_{i,\mathrm{AD}}^{(2\Delta)}} - \frac{\partial}{\partial x_j}\left(b^2 \frac{\partial}{\partial x_j}\overline{u_{i,\mathrm{AD}}^{(2\Delta)}}\right), \tag{3.2}$$

where $\overline{u_{i,\mathrm{AD}}^{(2\Delta)}} = u_i^{(2\Delta)}$. The parameter b is related to the local filter-width size and is dynamically computed using the procedure based on SGS kinetic energy matching described in Park *et al.* (2017). When the model is recursively applied, the model parameter b is not recomputed. Instead, the dimensionless parameter $b/(2\Delta)$ is kept constant across the reconstruction levels.

3.1.2. *Interpolation onto the finer grid*

The approximately-deconvolved velocity $u_{i,\mathrm{AD}}^{(2\Delta)}$ is interpolated onto the finer grid to obtain $u_{i,\mathrm{ADI}}^{(\Delta)}$. This step does not intentionally regenerate small scales with significant energy but nonetheless raises some numerical challenges that are worth discussing. First, note that low-order interpolating kernels behave as spatial filters. As a result, their utilization leads to artificial smoothing of the resolved velocity fluctuations that hinder the conservation of kinetic energy, which represents a quantity that plays a critical role in subsequent steps of the modeling approach outlined below. This issue is more severe in three-dimensional staggered grids where a refinement of the control volumes by a factor of 2 in each direction implies that none of the nodes of the original grid coincide with the nodes of the fine grid. The trilinear interpolation used in this work is observed to decrease the kinetic energy by 20% (see Section 4.1 for more details on the computational set-up). In this report, this issue is partly mitigated by adding an extra deconvolution step after interpolation in order to cancel the decrease in kinetic energy. This extra deconvolution step uses the DF model (3.2) described above, where the value of $b/(2\Delta)$ is chosen to be 0.82. This particular value is theoretically derived to enforce the condition that the spectral transfer function of a one-dimensional midpoint trilinear interpolation kernel matches the spectral transfer function of the differential filter at the dimensionless wavenumber $\pi/4$.

3.2. *Computation of* $u_{i,\mathrm{SGS}}^{(\Delta)}$

The interpolated velocity $u_{i,\mathrm{ADI}}^{(\Delta)}$ does not entail any significant SGS motion. The latter is diverted to $u_{i,\mathrm{SGS}}^{(\Delta)}$ by using the model expression

$$u_{i,\mathrm{SGS}}^{(\Delta)} = \sqrt{2K} \times \left(D_i / \sqrt{D_j D_j} \right). \tag{3.3}$$

This model is composed of two multiplicative terms that involve the square root of the local kinetic energy $K = u_{i,\mathrm{SGS}}^{(\Delta)} u_{i,\mathrm{SGS}}^{(\Delta)}/2$ based on the SGS velocity, and the normalized vector $D_i/\sqrt{D_j D_j}$ that models the structure of the SGS motion and relative magnitude of each velocity component, with D_i the local instantaneous growth-rate vector. The treatment of these two components is described in what follows.

3.2.1. *Computation of* D_i

The growth-rate vector of the subgrid scale motion is modeled as

$$D_i = N_i - \widetilde{N_i}, \tag{3.4}$$

where N_i is given by

$$N_i = \left[u_{j,\mathrm{ADI}}^{(\Delta)} - \widetilde{u_{j,\mathrm{ADI}}^{(\Delta)}} \right] \frac{\partial u_{i,\mathrm{ADI}}^{(\Delta)}}{\partial x_j} \tag{3.5}$$

and $\widetilde{(\cdot)}$ denotes a spatial filter with characteristic width 4Δ (i.e., twice as coarse as the LES grid). In Eq. (3.4), $\widetilde{N}_i$ is subtracted from N_i to avoid the modification of the resolved portion of N_i. The model form for the SGS velocity $u_{i,\mathrm{SGS}}^{(\Delta)}$ obtained by combining Eqs. (3.3)-(3.5) may reminisce the physical mechanism of generation of small scales by convection of large scales in turbulent flows. However, it models neither the pressure and viscosity effects on the generation or suppression of small scales, nor the time dynamics inherent to the generation process. Instead, the present model assumes that the subgrid

scales are instantaneously generated by one round of interactions among the resolved scales. Although the model is similar to the velocity estimation model of Domaradzki & Loh (1999) for the SGS stress, the present work reformulates it in the form given by Eq. (3.3), uses a different approximate-deconvolution scheme, and establishes dynamic procedures for the computation of the parameters involved in the model, including the prefactor $\sqrt{2K}$ in Eq. (3.3), as described below.

3.2.2. *Dynamic computation of K*

The local kinetic energy $K = u^{(\Delta)}_{i,\mathrm{SGS}} u^{(\Delta)}_{i,\mathrm{SGS}}/2$ based on the SGS velocity is estimated assuming that the kinetic energy of the small scales is proportional to that of the smallest resolved scales. This assumption resembles local self-similarity and leads to

$$K = K_{1,2} = C K_{2,4}, \tag{3.6}$$

where C is a proportionality constant that is dynamically computed as

$$C = \langle K_{2,4} \rangle / \langle K_{4,8} \rangle. \tag{3.7}$$

In Eq. (3.7), the angle brackets denote averaging along homogeneous directions. If the latter are not present in a particular flow configuration, the angle brackets are substituted by a series of filtering operations to regularize the dynamic constant, as traditionally performed in LES dynamic procedures. In the above formulation, $K_{m,n}$ denotes the kinetic energy of eddies whose sizes range from $m\Delta$ to $n\Delta$, namely

$$K_{2,4} = \left(u^{(\Delta)}_{i,\mathrm{ADI}} - \widetilde{u^{(\Delta)}_{i,\mathrm{ADI}}} \right) \left(u^{(\Delta)}_{i,\mathrm{ADI}} - \widetilde{u^{(\Delta)}_{i,\mathrm{ADI}}} \right) /2 \tag{3.8}$$

and

$$K_{4,8} = \left(\widetilde{u^{(\Delta)}_{i,\mathrm{ADI}}} - \widehat{u^{(\Delta)}_{i,\mathrm{ADI}}} \right) \left(\widetilde{u^{(\Delta)}_{i,\mathrm{ADI}}} - \widehat{u^{(\Delta)}_{i,\mathrm{ADI}}} \right) /2, \tag{3.9}$$

where $\widehat{(\cdot)}$ denotes a spatial filter with characteristic width 8Δ.

The motivation for the above dynamic procedure is perhaps best explained by making use of a power-like law for the kinetic-energy spectrum, $E_k(\kappa) \sim \kappa^{-\beta}$, where κ is the wavenumber and β is an exponent. It directly follows from this assumption that the ratio $K_{m,2m}/K_{2m,4m}$ is equal to a constant C independent of m. A sharp-spectral field yields a ratio equal to $2^{-\beta+1}$. Note that β can be imposed, for instance, using Kolmogorov's scaling $\beta = 5/3$, thereby leading to $C = 0.63$. Instead, the present model does not explictly require any value of β since the formulation uses a dynamic computation of C, as in Eq. (3.6). The value of β is indirectly is computed dynamically using the fact that it does not depend on m, as implied by Eq. (3.6). The scale-similarity assumption regarding the ratio of kinetic energies being independent of the specific wavenumber band becomes increasingly more unjustified near and within the viscous range, where the kinetic-energy spectrum no longer varies as a power law but rather does it exponentially. The larger the Reynolds number, the longer the inertial range is and the larger the number of reconstruction steps are that can be performed with the SDF model without incursions in the viscous range.

4. Numerical results

In this section, results obtained from the application of the SDF model to one-way coupled, homogeneous-isotropic particle-laden turbulence are described. The focus of the

analysis is on the impact of the SDF model on preferential-concentration statistics, which are known to be largely dominated by the small-scale eddies.

4.1. *Computational set-up*

The filtered conservation equations (1.1)-(1.2) are solved in a triply-periodic cubic domain using a finite-difference solver that employs second-order accurate in space and fourth-order accurate in time numerical schemes. The solver is described in Esmaily-Moghadam & Mani (2016). Constant-energy linear forcing is applied to the right-hand side of the momentum equation (1.2) in order to sustain the turbulence and achieve statistical stationarity (Bassenne *et al.* 2016). The Reynolds number based on the Taylor microscale is $\mathrm{Re}_\lambda = 85$. Besides LES, the analysis includes DNS of the unfiltered versions of the conservation equations (1.1)-(1.2) also at $\mathrm{Re}_\lambda = 85$ for comparisons. The maximum grid resolutions in DNS and LES are $\kappa_{\max}\ell_k = 1.5$ and $\kappa_{\max}\ell_k = 0.13$, respectively, with $\kappa_{\max} = \pi/\Delta$ being the largest wavenumber resolved by the grid in each case. The Kolmogorov length is $\ell_k = (\nu^3/\epsilon)^{1/4}$, where ν is the kinematic viscosity and ϵ is the mean molecular dissipation. This corresponds to a total number of 256^3 and 32^3 control volumes for DNS and LES, respectively. The SGS stress tensor is modeled in LES using the dynamic Smagorinsky model (Germano *et al.* 1991), where the dynamic constant is calculated using the least-squares approach of Lilly (1992). The physical parameters used in these simulations are similar to those in Park *et al.* (2017). All spatial filters are chosen to be box filters numerically implemented with a fourth-order Simpson rule for quadrature.

A large number of particles $N_p = 5 \times 256^3$ are randomly seeded once the motion of the carrier phase has reached a statistically steady state. This large number of particles is chosen to enable a physically meaningful interpretation of the number-density spectra, as described in Section 4.3 and thoroughly discussed in Bassenne *et al.* (2017). Data collection starts after a time sufficiently long compared to the characteristic particle acceleration time and to the time required for preferential-concentration statistics to become stationary (Jin *et al.* 2010). Specifically, time-averaged statistics are computed from 20 snapshots recorded during $14t_\ell$, with $t_\ell = \ell/u_\ell$ the integral time calculated using the associated integral length ℓ and fluctuation velocity u_ℓ. The motion of the particles is highly dependent on the Stokes number

$$\mathrm{St}_k = t_a/t_k, \tag{4.1}$$

whose values span from 2^{-2} to 2^3 with a power increment of one, with $t_k = \ell_k^2/\nu$ the Kolmogorov turnover time.

At every substep of the time-advancement scheme, the full-scale velocity u_i in Eq. (1.4) can be set equal to (a) the DNS velocity (denoted as DNS in the set of results presented below), (b) the resolved velocity $\overline{u}_i$ (LES), (c) the approximately-deconvolved velocity obtained from the dynamic DF model (LES-DF) in Park *et al.* (2015, 2017), or (d) the SDF-modeled velocity computed from Eq. (3.1) with one (LES-SDF1), two (LES-SDF2) or three (LES-SDF3) levels of reconstruction. The three alternatives in (d) amount to recovering a velocity field on a grid with 64^3, 128^3 or 256^3 control volumes, respectively. In the present work, the SDF-modeled velocity is solely used for integrating the particle equation of motion (1.4). Investigations of the utilization of the SDF-modeled velocity with the objective of computing the unclosed SGS stress in Eq. (1.2) are deferred to future work.

In its current form, the SDF model does not preserve the divergence of the original

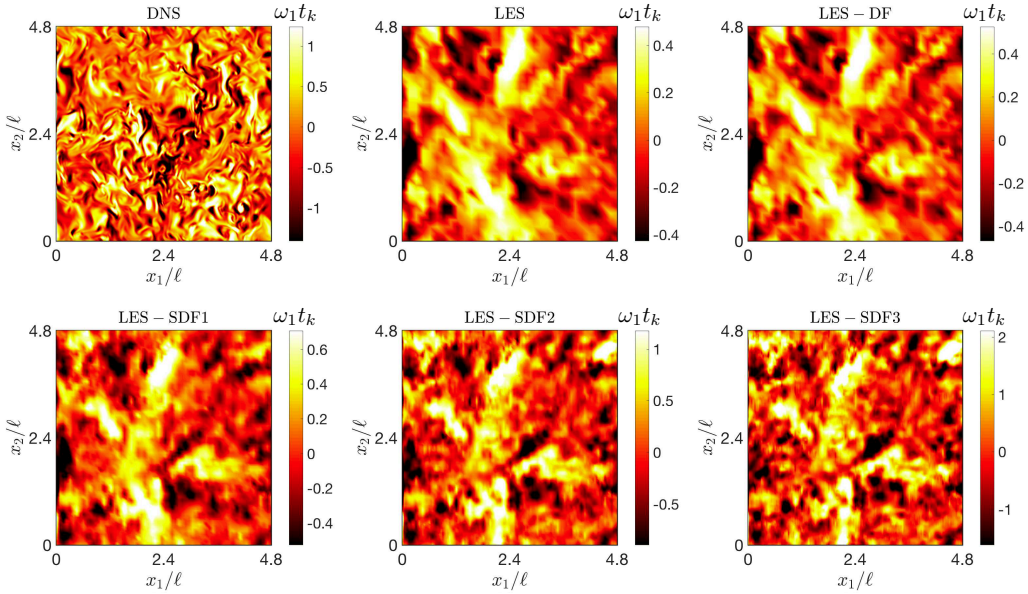

FIGURE 2. Instantaneous mid-plane cross sections of the x_1 component of the carrier-phase vorticity normalized with $1/t_k$, including DNS on a 256^3 grid (upper left panel) and LES on a 32^3 grid (upper center panel). The rest of the panels include the modeled x_1 component of the carrier-phase vorticity for the DF and SDF models on a grid corresponding to the reconstruction level. The extrema of the color maps are chosen to represent the 2.5% and 97.5% percentiles of the vorticity.

LES field. In this report, the divergence-free constraint is imposed on the velocities $u_{i,\mathrm{ADI}}^{(\Delta)}$ and $u_{i,\mathrm{SGS}}^{(\Delta)}$ at each reconstruction level. It is worth noting that imposing this constraint requires solving a Poisson-like linear system of equations on grids finer than the original LES grid, thereby increasing the overall computational cost of the model. Further work is required to either explore the conditions under which such corrections may not be relevant, or to perform modifications in the SDF-model algorithm with the objective of preserving the divergence-free condition without the need for solving the additional linear system of equations mentioned above. Note that the DF-modeled velocity field generally may not render zero divergence in a discrete sense even though the incompressibility condition is satisfied by the continuous formulation of the model when b is uniform. However, for consistency in the comparisons between LES-SDF and LES-DF, the zero-divergence constraint is also imposed on the LES-DF computations.

4.2. *Carrier-phase statistics*

The dynamic procedures described in Sections 3.1.1 and 3.2.2 yield reasonable values for the dynamic constants b and C. For instance, $b/(2\Delta) = 0.42$ on average, which is consistent with the value reported in Park *et al.* (2017). Similarly, the time-averaged values of C are 0.58, 0.27 and 0.14 for the first, second and third levels of reconstruction, respectively. These values are of the same order as 0.63, which corresponds to the value obtained with the assumption of Kolmogorov $-5/3$ scaling for the kinetic-energy spectrum (i.e., see Section 3.2.2). Note however that, as the number of reconstruction levels increases, C deviates from the value 0.63 estimated from the Kolmogorov scaling. This occurs because the dynamic procedure becomes increasingly biased by modeling errors

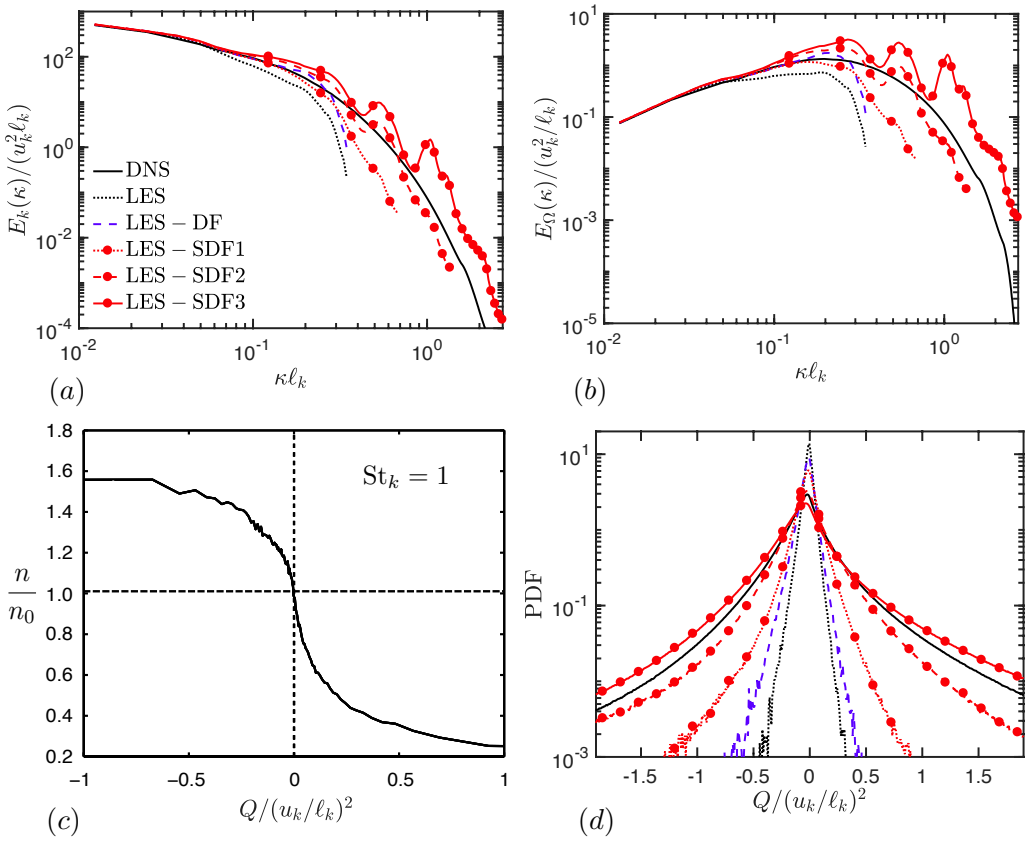

FIGURE 3. Carrier-phase ensemble-averaged Fourier spectra of (a) turbulent kinetic energy and (b) enstrophy. The figure also includes (c) DNS conditional mean of the particle number density as a function of the normalized second invariant of the carrier-phase velocity-gradient tensor Q for unity Stokes numbers, and (d) ensemble-averaged PDF of Q. In panels (a), (b) and (d), the different curves correspond to DNS (256^3), LES (32^3), LES-DF (32^3), LES-SDF1 (64^3), LES-SDF2 (128^3) and LES-SDF3 (256^3) [see legend in panel (a) for line types].

as the reconstruction level increases, and because the wavenumber extent of the inertial subrange is rather limited in these simulations.

The instantaneous cross sections of the carrier-phase vorticity component ω_1 are shown in Figure 2. As usual, the DNS contours contain fine-grained vortical features that are absent in the much coarser LES. Similarly, the LES-DF contours do not encompass vortical structures smaller than those already observed in the LES as a result of the lack of spectral enrichment in approximate-deconvolution models. However, the existing eddies with a size similar to that of the LES grid resolution are amplified in LES-DF (Park *et al.* 2017). In contrast, the LES-SDF contours show qualitative evidence that the SDF model incorporates small vortical structures. As the number of reconstruction levels increases from one to three, the modeled vorticity becomes increasingly more populated at high wavenumbers.

A similar effect is quantitatively observed in the spectra of the turbulent kinetic energy and enstrophy of the carrier phase, which are shown in Figure 3(a,b). While the spectra in LES and LES-DF have the same support in wavenumber space, the LES-SDF spectra

have increased support as the number of reconstruction levels is increased since the SDF-modeled velocity field is defined on a finer grid. An additional observation worth remarking in Figure 3(a,b) is that the LES-SDF1 spectrum lies below the LES-DF one. Further analysis shows that this is due to the energy loss induced by the interpolation scheme, as described in Section 3.1.2. The second deconvolution step is not sufficient to compensate the numerical dissipation induced by the interpolation. Furthermore, the LES-SDF spectra exhibit spurious oscillations caused by the low-order interpolation scheme used in this study and the dyadic-based reconstruction of the velocity. Future work will involve the use of higher-order interpolation schemes in order to suppress these spurious oscillations.

A quantity of interest in particle-laden turbulence is the second invariant of the velocity-gradient tensor Q. In the limit of small Stokes numbers, particles cluster in straining regions (i.e., $Q < 0$) and are centrifuged away from vortical regions (i.e., $Q > 0$) (Robinson 1956; Maxey 1987; Esmaily-Moghadam & Mani 2016). This is illustrated in Figure 3(c), which shows the resulting anti-correlation between the conditional mean of the particle number density and Q in DNS. It is therefore evident that the prediction of the particle concentration field heavily relies on the prediction of the Q field. However, as observed in Figure 2, LES tends to underpredict vortical intermittency, and as a result, leads to exceedingly narrow PDFs of Q when compared to DNS, as shown in Figure 3(d). In contrast, increasingly improved predictions are obtained by using LES-DF, LES-SDF1, LES-SDF2 and LES-SDF3. Remarkably, the LES-SDF3, whose modeled velocity is defined on a grid that has the same resolution as the DNS grid, closely reproduces the tails of the PDF of Q observed in the DNS results.

4.3. *Dispersed-phase statistics*

Ensemble-averaged radial distribution functions (RDFs), which quantify the likelihood that a given pair of particles is separated by a certain radial distance [e.g., see Ray & Collins (2011) for further details], are shown in Figure 4. Comparisons between DNS and LES results show that LES underpredicts particle clustering when the Stokes number is smaller than unity, while an overprediction occurs in the opposite limit of large Stokes numbers. This poses a challenge for SGS models attempting to predict preferential concentration, in that they should be able to counteract the LES mismatches by steering the particles in a different way on each side of the $\mathrm{St}_k \sim 1$ limit. Specifically, at small Stokes numbers the SGS-modeled velocity should cluster or anti-disperse the particles. Conversely, at large Stokes numbers the SGS-modeled velocity should disperse the particles. Remarkably, the LES-DF and LES-SDF results in Figure 4 show that both the non-spectrally enriched DF model in Park *et al.* (2015, 2017) and the spectrally-enriched DF model proposed here consistently reproduce the anti-dispersion and dispersion trends required for $\mathrm{St}_k \ll 1$ and $\mathrm{St}_k \gg 1$, respectively. Nonetheless, LES-DF does not fully recover the RDFs observed in DNS because of the insufficient level of intermittency in the velocity gradients. In contrast, the predictions are greatly improved in LES-SDF, with an increasing agreement being observed as the number of reconstruction levels increases from one to three with exception of the unity Stokes-number case, which remains under investigation. In all other cases, the order of predictive capability is LES, LES-DF, LES-SDF1, LES-SDF2, LES-SDF3 and DNS. As the Stokes number is increased, the advantages of deploying an additional level of reconstruction in the LES-SDF model becomes less clear, since the particles become increasingly inertial to the small scales regenerated by the model.

In order to address the performance of the SDF model in predicting the scales and fluctuation intensity associated with the particle concentration field, Figure 5 shows the

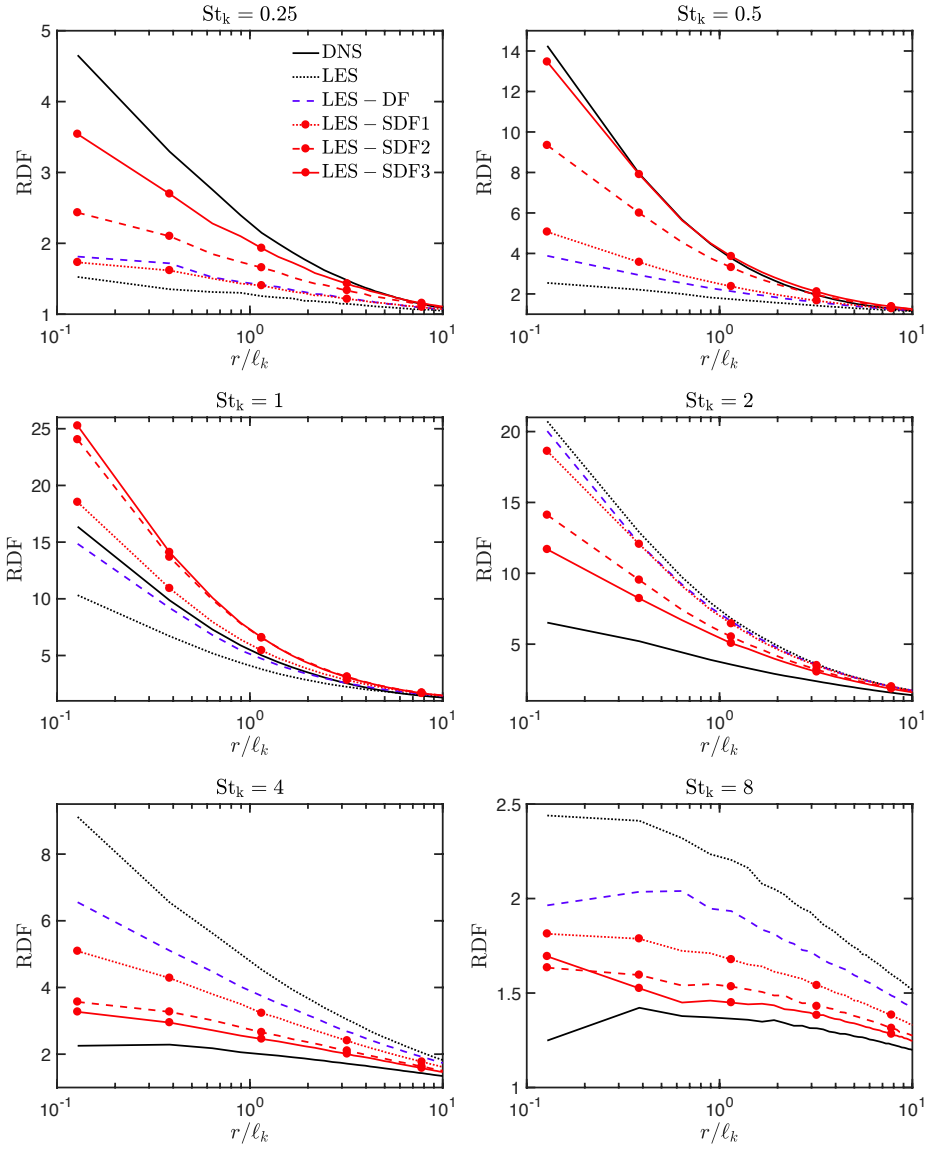

FIGURE 4. Ensemble-averaged radial distribution functions (RDFs) for different Stokes numbers and SGS velocity models.

energy spectra of the particle number-density fluctuations. A description of the physical meaning of these spectra in DNS, LES and LES-DF for a wide range of Stokes numbers is provided in Park *et al.* (2017). While the spectra peak at resolved wavenumbers at large Stokes numbers, the contrary occurs at small or near-unity Stokes numbers. In the absence of appropriate spectral support, the LES results lead to important disagreements with DNS. At large Stokes numbers, the magnitude of the spectrum peak is overpredicted by LES but its location in the wavenumber axis is well reproduced. Significant improve-

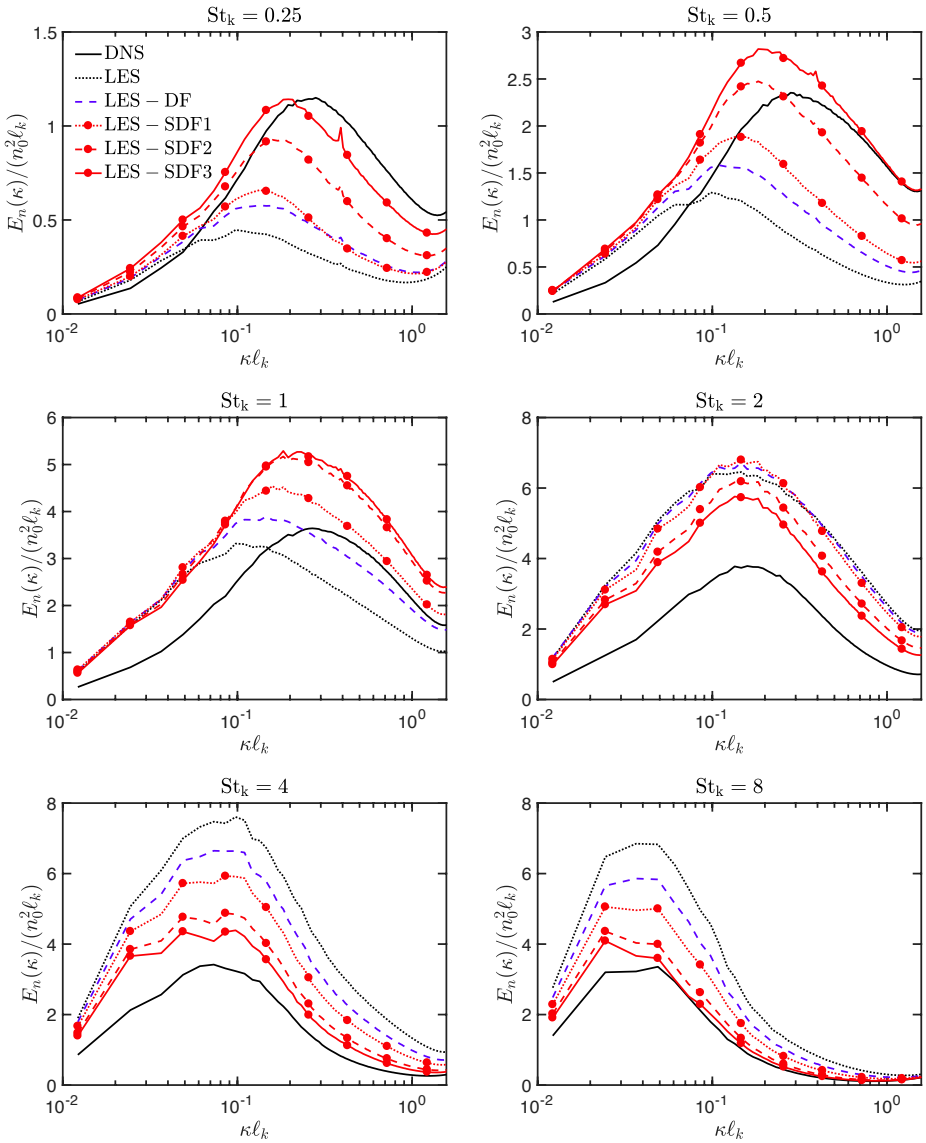

FIGURE 5. Ensemble-averaged number-density Fourier spectra for different Stokes numbers and SGS velocity models. The LES wavenumber cutoff is located at $\kappa\ell_k = 0.13$.

ments are observed when LES-DF and LES-SDF are employed, the latter rendering the best results in the third level of reconstruction. Conversely, at Stokes numbers smaller than unity, both LES and LES-DF miscalculate the location of the spectrum peak, which is artificially shifted toward larger scales as a result of the inaccessibility of LES to sub-grid wavenumbers. However, the LES-SDF model considerably improves the prediction of the spectra at scales smaller than the original LES grid while capturing increasingly more accurately the shift in the peak location and the peak magnitude as the level of reconstruction is increased. The considerations given above are ratified by visualizing

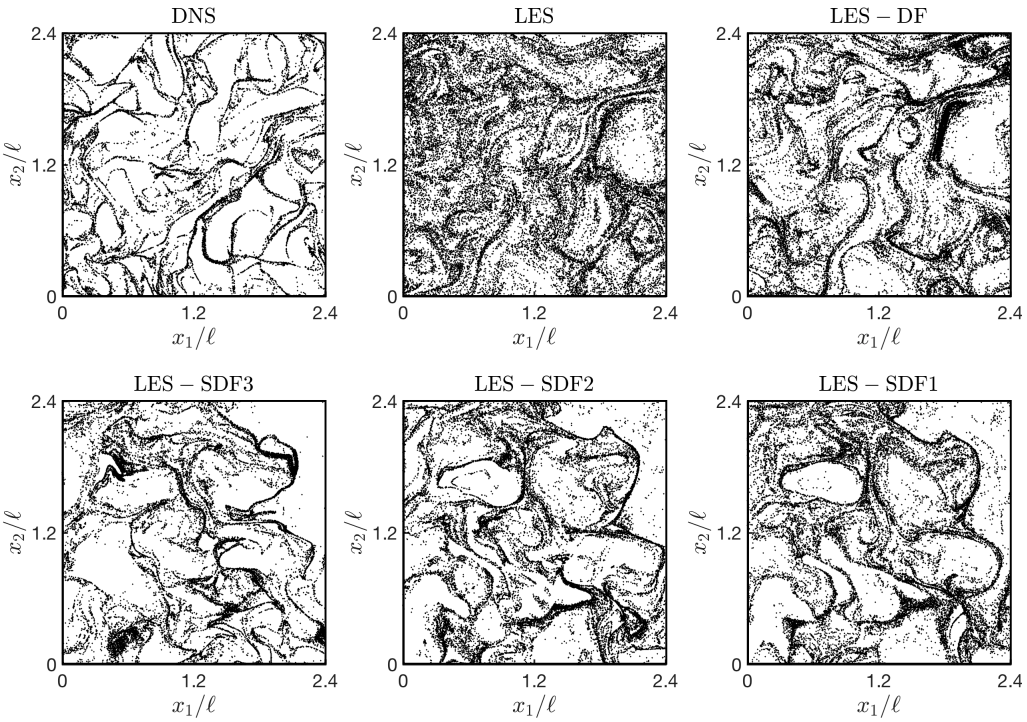

FIGURE 6. Instantaneous spatial distribution of particles (dots) contained in a slice of thickness ℓ_k for $\mathrm{St}_k = 0.5$. Only half of the computational domain in the x_1 and x_2 directions is represented for clarity.

the spatial distribution of particles in Figures 6 and 7. Specifically, the visualizations confirm that the LES-SDF model increasingly improves the performance compared to LES and LES-DF as the number of reconstruction level is increased, both in terms of predicting the overall structure of the preferentially concentrated clouds of particles and their associated spatial scales.

5. Conclusions

In this work, a new subgrid-scale model for LES of particle-laden turbulence formulated in physical space is proposed, which constructs an spectrally-enriched velocity field on a grid finer than the original LES grid. The model extends the dynamic DF model of Park *et al.* (2017) using a dynamic re-formulation of the velocity estimation model by Domaradzki & Loh (1999). The procedure for regenerating SGS motion from the resolved velocity field does not entail tunable parameters. The regeneration of small scales in the model is based on non-linear, convective interactions between resolved eddies.

The model performance is assessed in homogeneous-isotropic turbulence laden with a dilute suspension of inertial point particles. In most cases, the prediction of preferential concentration is improved compared to LES with no model and to LES with the dynamic DF model of Park *et al.* (2017). The intensity and scales of associated with the particle concentration field are better predicted with the new model since it bears scales smaller than the LES grid cutoff. The model is also shown to increasingly reproduce the

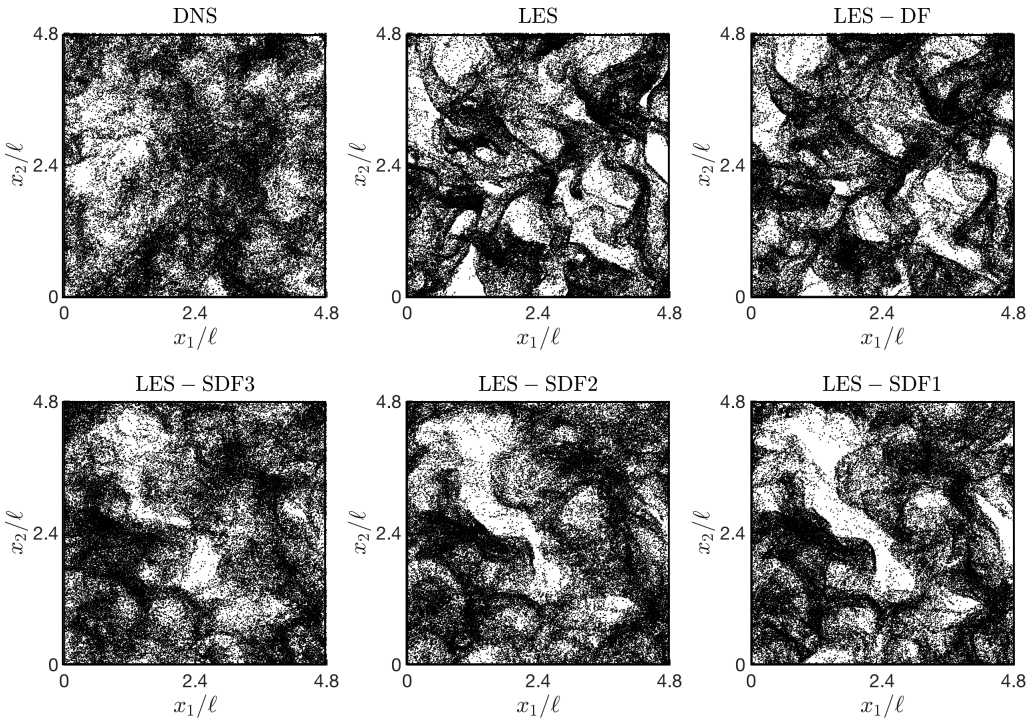

FIGURE 7. Instantaneous spatial distribution of particles (dots) contained in a slice of thickness ℓ_k for $\mathrm{St}_k = 8$.

spatial intermittency of the carrier-phase velocity gradients as the reconstruction level is increased.

Future work may include the investigation of higher-order interpolation schemes for interpolating the carrier-phase velocity onto finer grids in the model formulation, the analysis of the structural properties of the SGS-modeled velocity field, and the extension of the assessment of the model to particle kinematics statistics in wall-bounded flows. In addition, analyses of the sensitivity of the results to the divergence of the modeled velocity field may be worthwhile since enforcing zero divergence requires to solve a linear system of equations that increases the computational cost of the model. This cost would further increase in complex geometries where the development of fast linear solvers is a subject of research. Lastly, it is worth mentioning that it is possible to use the present SGS model locally on a cell-by-cell basis, by reconstructing an spectrally-enriched velocity field in physical space only in spatial regions characterized, for instance, by high concentration of particles, in a way similar to that proposed within the context of conceptual PP-CCS models discussed in Section 2.3.

Acknowledgments

The authors are grateful to Dr. Sanjeeb Bose and Dr. Perry Johnson for useful discussions. This investigation was funded by the Advanced Simulation and Computing (ASC) program of the US Department of Energys National Nuclear Security Administration via the PSAAP-II Center at Stanford, Grant #DE-NA0002373. The first author is grateful

to LANL for the hospitality during his stay in Summer 2017 as part of the PSAAP-II student visiting program.

REFERENCES

Bassenne, M., Urzay, J. & Moin, P. 2015 Spatially-localized wavelet-based spectral analysis of preferential concentration in particle-laden turbulence. *Annual Research Briefs*, Center for Turbulence Research, Stanford University, pp. 3-16.

Bassenne, M., Urzay, J., Park, G. I. & Moin, P. 2016 Constant-energetics physical-space forcing methods for improved convergence to homogeneous-isotropic turbulence with application to particle-laden flows. *Phys. Fluids* **28**, 035114.

Bassenne, M., Urzay, J. & Moin, P. 2017 Extraction of coherent clusters and grid adaptation in particle-laden turbulence using wavelet filters. *Phys. Rev. Fluids* **2**, 054301.

Bürger, K., Treib, M., Westermann, R., Werner, S., Lalescu, C. C., Szalay, A., Meneveau, C. & Eyink, G. L. 2013 Vortices within vortices: hierarchical nature of vortex tubes in turbulence. In arXiv preprint, arXiv:1210.3325v2.

Domaradzki, J. A. & Loh, K. 1999 The subgrid-scale estimation model in the physical space representation. *Phys. Fluids* **11**, 2330–2342.

Esmaily-Moghadam, M. & Mani, A. 2016 Analysis of the clustering of inertial particles in turbulent flows. *Phys. Rev. Fluids* **1**, 084202.

Ferrante, A. & Elghobashi, S. 2003 On the physical mechanisms of two-way coupling in particle-laden isotropic turbulence. *Phys. Fluids* **15**, 315–329.

Germano, M., Piomelli, U., Moin, P. & Cabot, W. 1991 A dynamic subgrid-scale eddy viscosity model. *Phys. Fluids* **3**, 1760–1765.

Gobert, C. & Manhart, M. 2011 Subgrid modelling for particles-LES by spectrally optimised interpolation. *J. Comput. Phys.* **230**, 7796–7820.

He, G., Jin, G. & Yang, Y. 2017 Space-time correlations and dynamic coupling in turbulent flows. *Annu. Rev. Fluid Mech.* **49**, 51–70.

Jiménez, J., Wray, A. A., Saffman, P. G. & Rogallo, R. S. 1993 The structure of intense vorticity in isotropic turbulence. *J. Fluid Mech.* **255**, 65–90.

Jin, G., He, G. W. & Wang, L. P. 2010 Large-eddy simulation of turbulent collision of heavy particles in isotropic turbulence. *Phys. Fluids* **22**, 055106.

Lilly, D. K. 1992 A proposed modification of the Germano subgrid-scale closure method. *Phys. Fluids* **4**, 633–635.

Marchioli, C. 2017 Large-eddy simulation of turbulent dispersed flows: a review of modelling approaches. *Acta Mech.* **228**, 741–771.

Marchioli, C., Salvetti, M. & Soldati, A. 2008*a* Some issues concerning large-eddy simulation of inertial particle dispersion in turbulent bounded flows. *Phys. Fluids* **20**, 040603.

Marchioli, C., Salvetti, M. V. & Soldati, A. 2008*b* Appraisal of energy recovering sub-grid scale models for large-eddy simulation of turbulent dispersed flows. *Acta Mech.* **201**, 277–296.

Maxey, M. R. 1987 The gravitational settling of aerosol particles in homogeneous turbulence and random flow fields. *J. Fluid Mech.* **174**, 441–465.

Maxey, M. R. & Riley, J. J. 1983 Equation of motion for a small rigid sphere in a nonuniform flow. *Phys. Fluids* **26**, 883–889.

Mazzitelli, I. M., Toschi, F. & Lanotte, A. S. 2014 An accurate and efficient Lagrangian sub-grid model. *Phys. Fluids* **26**, 095101.

Minier, J. P. 2015 On Lagrangian stochastic methods for turbulent polydisperse two-phase reactive flows. *Prog. Energy Combust. Sci.* **50**, 1–62.

Murray, S., Lightstone, M. & Tullis, S. 2016 Single-particle Lagrangian and structure statistics in kinematically simulated particle-laden turbulent flows. *Phys. Fluids* **28**, 033302.

Park, G. I., Urzay, J., Bassenne, M. & Moin, P. 2015 A dynamic subgrid-scale model based on differential filters for LES of particle-laden turbulent flows. *Annual Research Briefs*, Center for Turbulence Research, Stanford University, pp. 17-26.

Park, G. I., Bassenne, M., Urzay, J. & Moin, P. 2017 A simple dynamic subgrid-scale model for LES of particle-laden turbulence. *Phys. Rev. Fluids* **2**, 044301.

Ray, B. & Collins, L. 2011 Preferential concentration and relative velocity statistics of inertial particles in Navier–Stokes turbulence with and without filtering. *J. Fluid Mech.* **680**, 488–510.

Ray, B. & Collins, L. 2014 A subgrid model for clustering of high-inertia particles in large-eddy simulations of turbulence. *J. Turbul.* **15**, 366–385.

Robinson, A. 1956 On the motion of small particles in a potential field of flow. *Comm. Pure Appl. Math* **9**, 69–84.

Schneider, K. & Vasilyev, O. 2010 Wavelet methods in computational fluid dynamics. *Annu. Rev. Fluid Mech.* **42**, 473–503.

Squires, K. D. & Eaton, J. K. 1991 Preferential concentration of particles by turbulence. *Phys. Fluids* **3**, 1169–1178.

Urzay, J., Bassenne, M., Park, G. I. & Moin, P. 2014 Characteristic regimes of subgrid-scale coupling in LES of particle-laden turbulent flows. *Annual Research Briefs*, Center for Turbulence Research, Stanford University, pp. 3–13.